

Supplementary Information

1

2

3 **Constructing heterogeneous asymmetric sites for highly-selective methane**
4 **production from CO₂ electroreduction**

5

6 *Yan Huang,^a Wen-Chuan Lai, ^{*a} and Zhi-Yuan Gu^a*

7

8 College of Chemistry and Materials Science, Nanjing Normal University, Nanjing, Jiangsu 210023,
9 P. R. China

10

11 Correspondence and requests for materials should be addressed to W. L. (laiwenchuan@nnu.edu.cn).

12 **1. Experimental Section**

13 **1.1 Chemicals**

14 All reagents were obtained commercially and no further purification was performed. Copper nitrate
15 trihydrate ($\text{Cu}(\text{NO}_3)_2 \cdot 3\text{H}_2\text{O}$) oxalic acid ($\text{C}_2\text{H}_2\text{O}_4$) and potassium chloride (KCl) were purchased
16 from Aladdin (Shanghai), China. Europium (III) acetate hydrate ($\text{C}_6\text{H}_9\text{EuO}_6$) was purchased from
17 Macklin (Shanghai), China. Anhydrous ethanol ($\text{C}_2\text{H}_5\text{OH}$) was purchased from Sinopod Chemical
18 Reagent Co., LTD. Toray Carbon Paper (TGP-H-60) and Nafion 117 proton exchange membrane and
19 Nafion D-521 dispersion (5 wt% in lower aliphatic alcohols and water) and were purchased from
20 Shanghai Hesens Electric Co., Ltd. The ultrapure water ($18.2 \text{ M}\Omega \cdot \text{cm}$) was prepared by an ELGA
21 purification system (Veolia Water Solutions & Technologies, UK). Water was from Wahaha prepared
22 by Wahaha Group Co., LTD., Hangzhou, China

23

24 **1.2 Synthesis of Eu/Cu-x (x=1-3)**

25 The Eu/Cu-x (x=1-3) catalysts were synthesized via a coprecipitation method followed by
26 calcination. In the preparation of Eu/Cu-2, 0.8 mmol of $\text{Cu}(\text{NO}_3)_2 \cdot 3\text{H}_2\text{O}$ and 1.1 mmol of $\text{C}_6\text{H}_9\text{EuO}_6$
27 were dissolved in 80 mL of deionized water under magnetic stirring at room temperature for 20 min.
28 Separately, 4.9 mmol of $\text{C}_2\text{H}_2\text{O}_4$ was dissolved in 30 mL of deionized water at 60°C until fully
29 dissolved. The oxalic acid solution was then gradually added to the metal salt mixture under vigorous
30 stirring for 1 hours (h). The resulting precipitate was washed three times with deionized water and
31 ethanol, respectively, and dried overnight at 80°C to obtain the Eu/Cu-oxalate-2 precursor. The
32 precursor was calcined in a muffle furnace by heating to 450°C at a rate of $2^\circ\text{C}/\text{min}$, maintained at
33 this temperature for 1 h, and then cooled to room temperature to yield the final metal oxide catalyst
34 (Eu/Cu-2). Catalysts with varying Eu/Cu-1 and Eu/Cu-1 were prepared using analogous procedures.
35 $\text{Cu}(\text{NO}_3)_2 \cdot 3\text{H}_2\text{O}$ was 0.8 mmol, $\text{C}_6\text{H}_9\text{EuO}_6$ as 0.4 mmol or 3.2 mmol, $\text{C}_2\text{H}_2\text{O}_4$ as 2.8 mmol or 11.2
36 mmol, respectively. The reference CuO catalyst was synthesized with 1.6 mmol $\text{C}_2\text{H}_2\text{O}_4$ without
37 adding $\text{C}_6\text{H}_9\text{EuO}_6$.

38

39 **1.3 Characterizations.**

40 Powder X-ray diffraction pattern (XRD) is an instrument (Japan) D/MAX-2500 Cu K α radiation
41 diffractometer ($\lambda=1.54056 \text{ \AA}$) obtained with Rigaku 9kw. The morphology of the materials was

42 characterized using scanning electron microscopy (SEM, JSM-7600 and Apreo 2S, JEOL Ltd, Japan)
43 and high-resolution transmission electron microscopy (HRTEM, JEM-2100F, 200 kV, JEOL, Japan).
44 X-ray photoelectron spectra were acquired using an ESCALAB Xi⁺ X-ray photoelectron spectrometer
45 (Thermo Fisher). ¹H NMR were acquired using an AVANCE III HD 400 (Bruker) for liquid phase
46 product quantification. Gas products were quantitatively analyzed using a gas chromatograph
47 (PANNA A91). All electrochemical data were acquired using Shanghai Chenhua CHI660E.

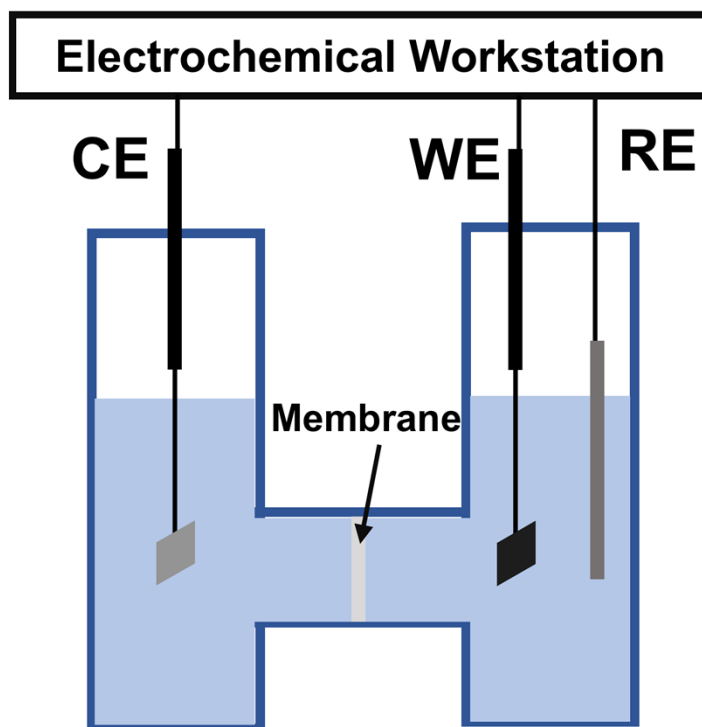
48

49 **1.4 Electrochemical Measurement**

50 Electrochemical measurements were conducted in a two-compartment H-cell equipped with a three-
51 electrode system, separated by a proton exchange membrane (Nafion 117). To prepare the working
52 electrode, 10 mg of catalyst was dispersed in 1000 μL ethanol and mixed with 100 μL of 5 wt%
53 Nafion solution. The mixture was ultrasonicated for 1 h to form the catalyst ink. Subsequently, the
54 ink was uniformly coated onto carbon paper (1×2 cm²), achieving a loading of 1 mg·cm⁻². The
55 Ag/AgCl electrode (3 M KCl) served as the reference electrode, and a 1×1 cm² Pt foil was employed
56 as the counter electrode. Prior to testing, the electrolyte (0.1 M KCl) was purged with CO₂ for 10 min
57 to ensure saturation. The eCO₂RR experiment was conducted in a CO₂-saturated electrolyte with
58 continuous CO₂ passage at a flow rate of 10 mL/min at room temperature. All potentials are reported
59 versus the reversible hydrogen electrode (RHE) without *i*R compensation, using the following
60 conversion formula:

$$61 \quad E(V_{\text{RHE}}) = E(V_{\text{Ag/AgCl}}) + 0.197\text{V} + 0.0591 \times \text{pH}$$

62 Gaseous products were detected by online gas chromatography every 10 min. The liquid products
63 were analyzed by ¹H NMR (Nuclear Magnetic Resonance).



64
65 **Fig. S1** schematic illustration of H-cell for eCO₂RR measurement.

66

67 1.5 Product Analysis

68 Gas chromatography (GC, PANNA, A91PLUS) was employed for the analysis of gaseous products
69 from eCO₂RR. The system utilized a flame ionization detector (FID) and a thermal conductivity
70 detector (TCD), with ultra-high purity nitrogen (99.999%) as the carrier gas. Each injection consisted
71 of 1 mL of gas sample. The effluent gas mixture from the reactor first passed through the TCD before
72 being analyzed by the FID.

73 The equation for calculating the FE for gaseous products is:

$$74 \quad FE(\%) = \frac{Q_{gas}}{Q_{total}} = \frac{nzF}{Q} = \frac{V \cdot vzF}{V_m \cdot I} \times 100\%$$

75 where V is the relative gas content read directly from the gas chromatograph; v is the flow rate of CO₂
76 output (L·s⁻¹); z is the electron transfer number of eCO₂RR product (different reduction products have
77 different electron transfer numbers); F is the Faraday constant (96485 C·mol⁻¹); V_m is the gas molar
78 volume (22.4 L·mol⁻¹) and I is the current (A) under standard conditions.

79 The equation for calculating the FE for liquid products is:

80
$$FE(\%) = \frac{Q_{liquid}}{Q_{total}} \times 100\% = \frac{n_{liquid}zF}{Q_{total}} 100\%$$

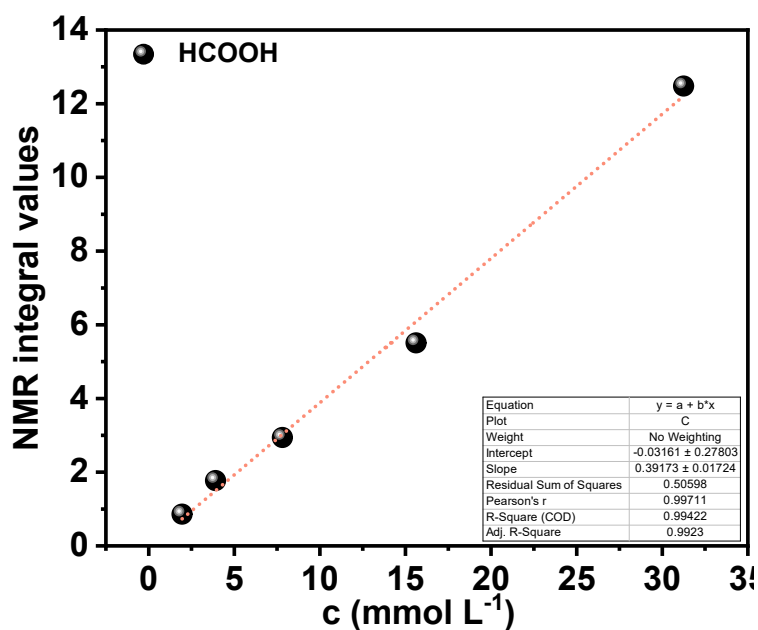
81 Where n_{liquid} is the amount of substance of the liquid product (mol); Q_{total} is the total charge (C).

82

83 1.6 Standard curves on NMR and GC.

84 The determination of HCOOH content is performed by quantifying HCOOH in liquid products

85 through the internal standard method. The standard curves are listed below.



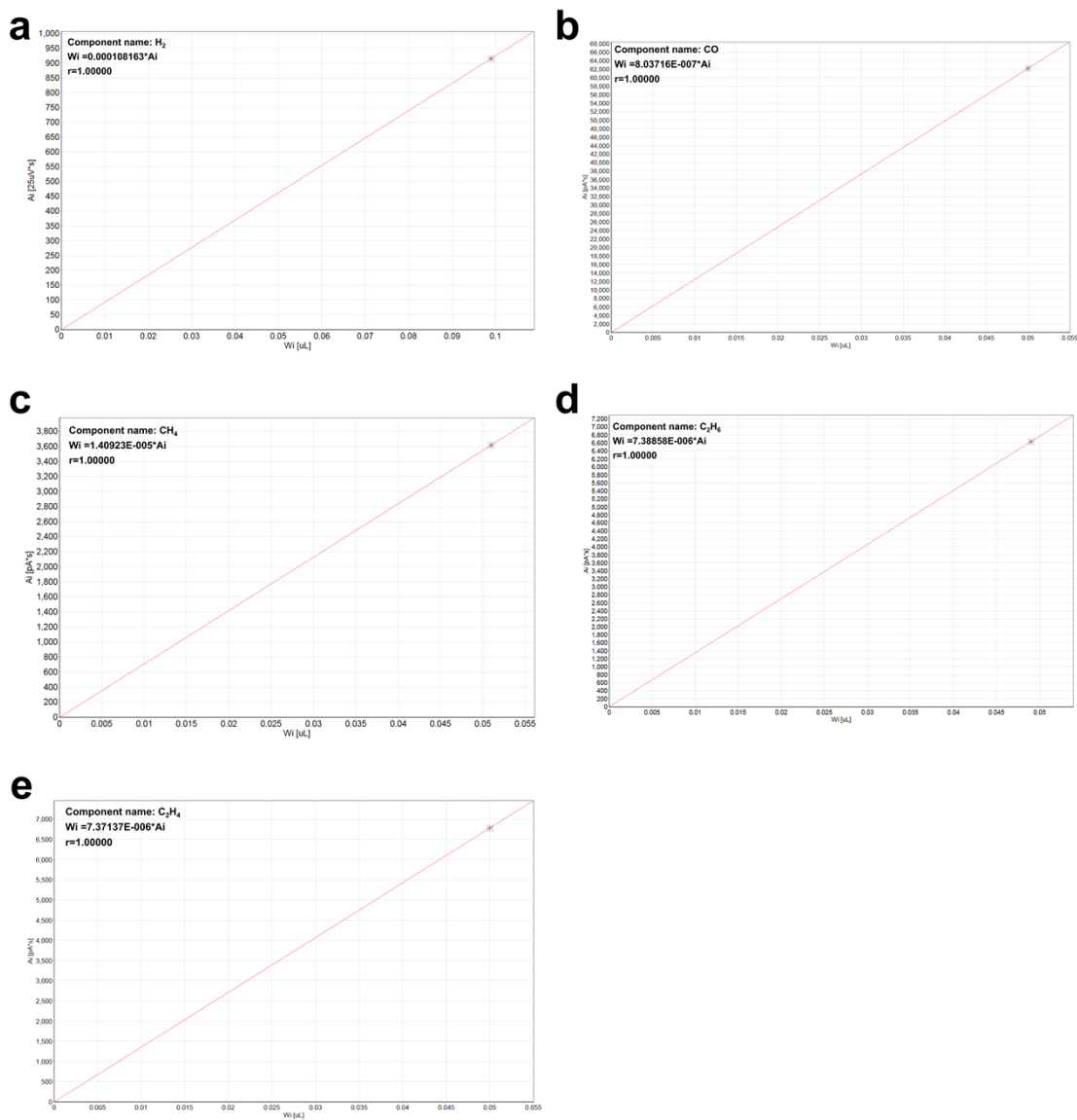
86

87

Fig. S2 The standard curves of HCOOH.

88 The standard curves of H_2 , CO, CH_4 , C_2H_4 , C_2H_6 , and C_3H_6 . H_2 and CO are detected by TCD and all

89 the hydrocarbons are detected by FID. High linearities ensure the reliability of our data.

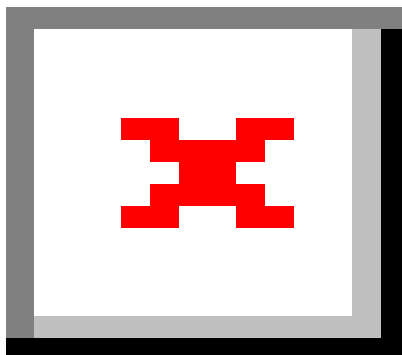


90

91

Fig. S3 The standard curves of (a) H₂, (b) CO, (c) CH₄, (d) C₂H₆, and (e) C₂H₄.

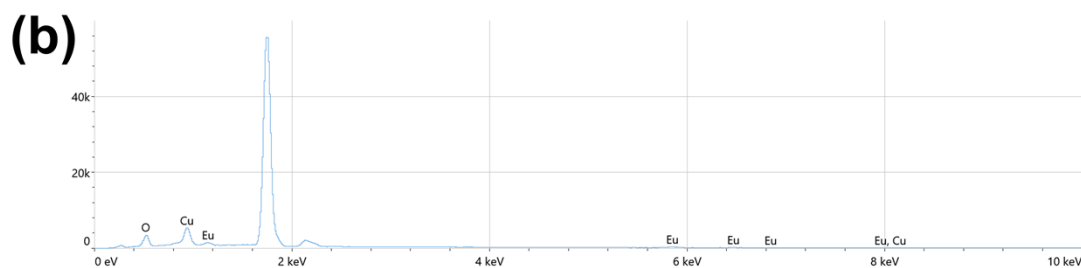
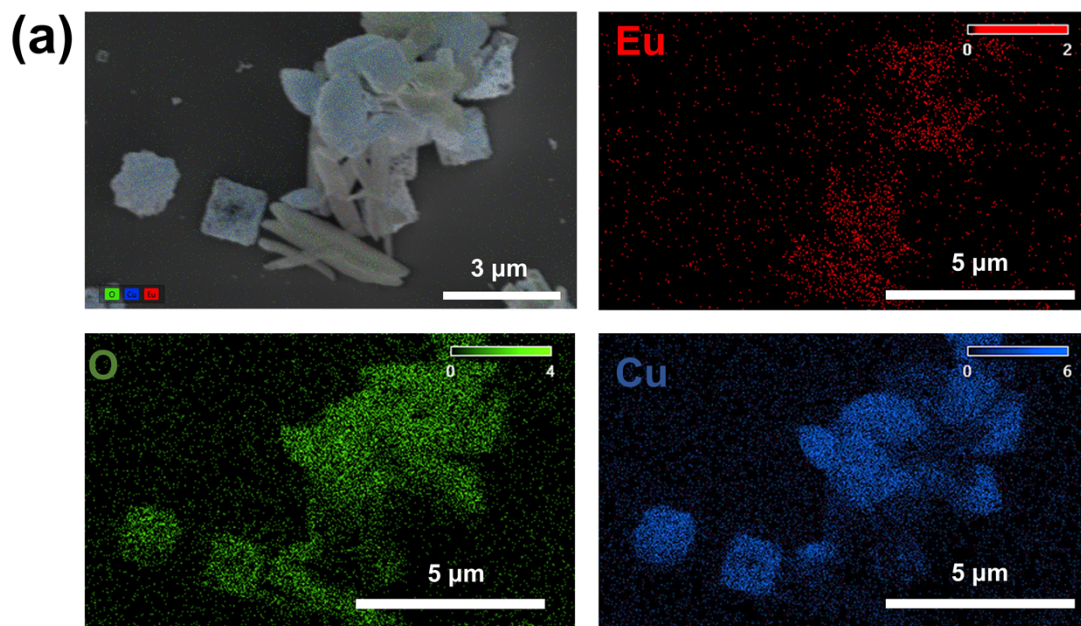
92 **2. Supplementary figures**



93

94 **Fig. S4** XRD pattern of CuC_2O_4 , Eu/Cu-oxalate-1, Eu/Cu-oxalate-2, Eu/Cu-oxalate-3.

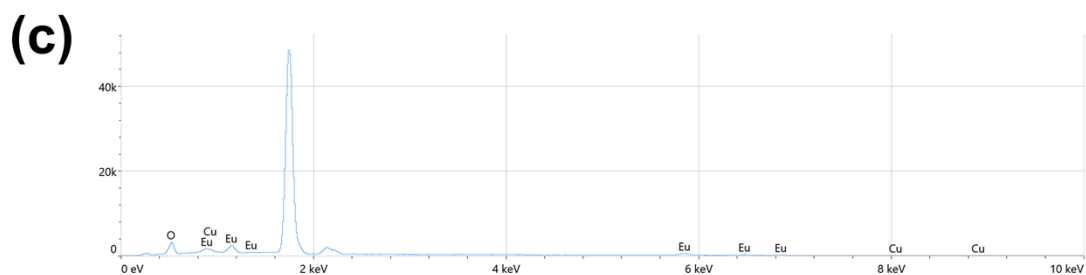
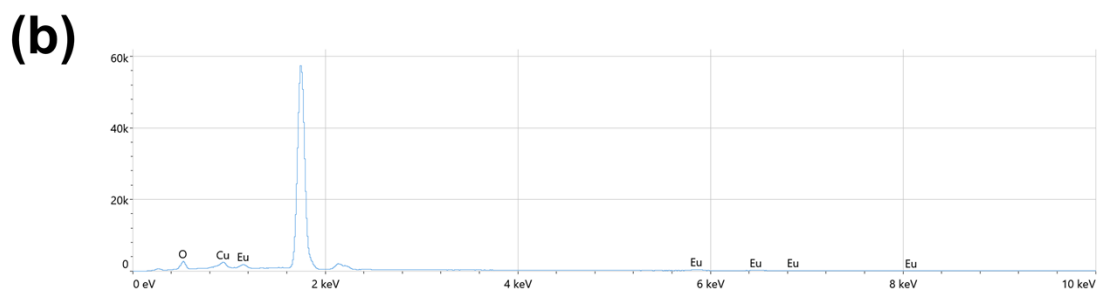
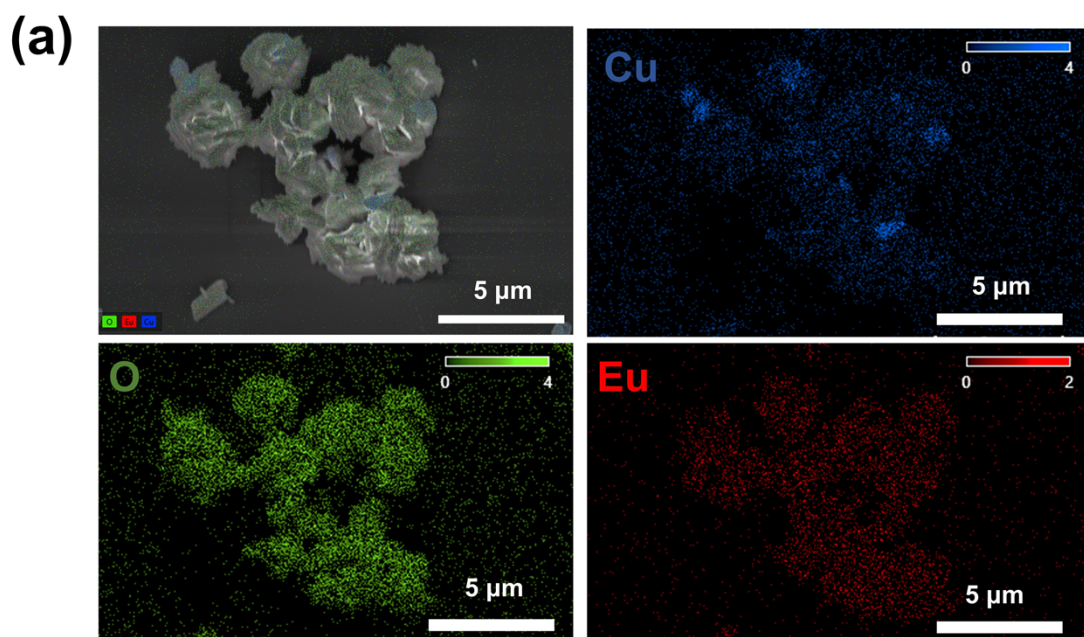
95



96

97 **Fig. S5** (a) EDS image of Eu/Cu-1. (b) The corresponding EDS indicating the atomic ratio in Eu/Cu-1.

98



99

100 **Fig. S6** (a) EDS image of Eu/Cu-3. (b) The corresponding EDS indicating the atomic ratio in Eu/Cu-2.

101 (c) The corresponding EDS indicating the atomic ratio in Eu/Cu-3.

102

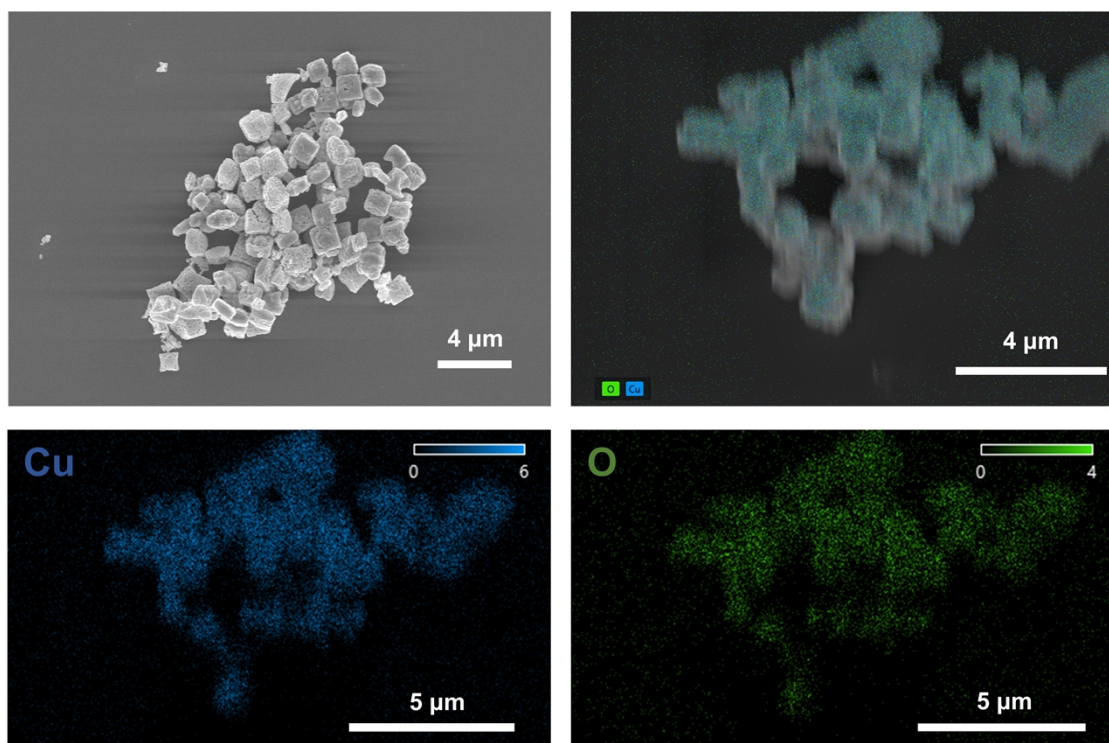
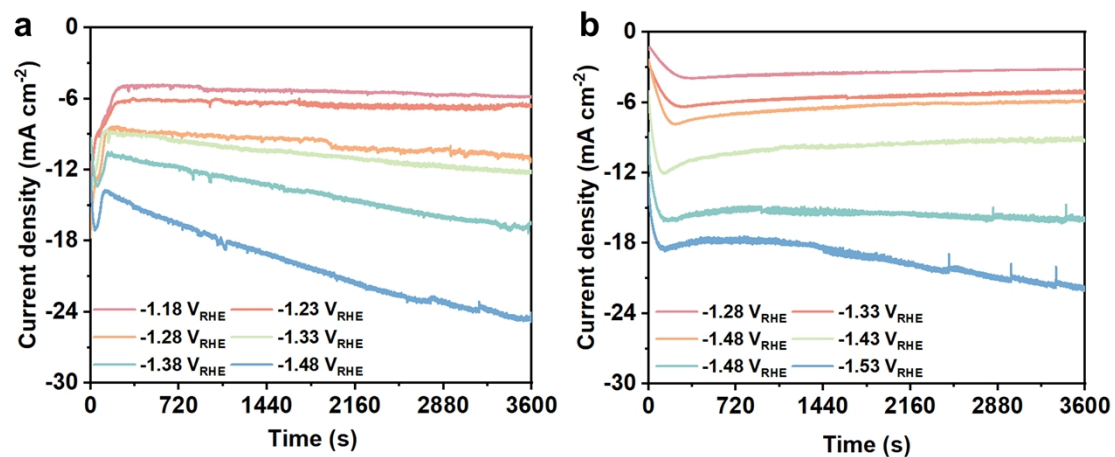


Fig. S7 EDS image of CuO.

103

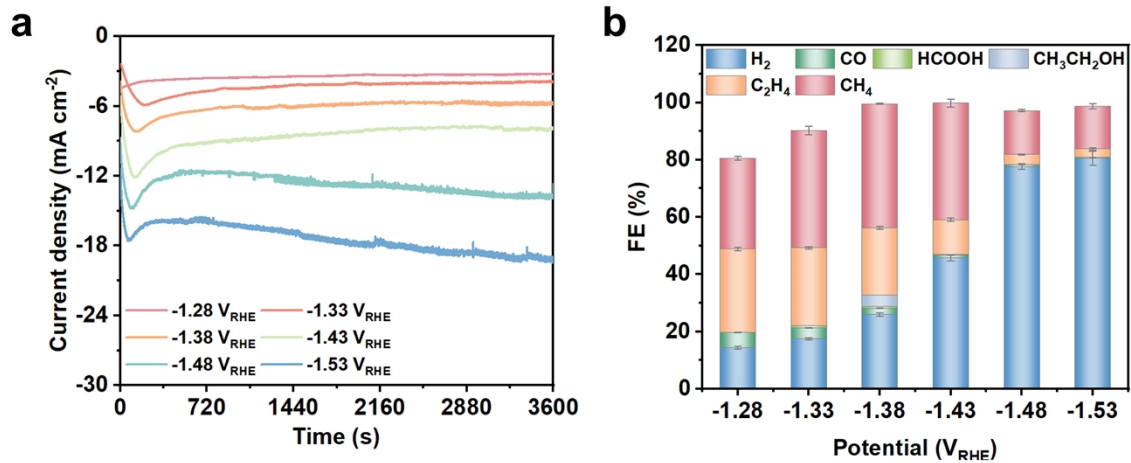
104



105

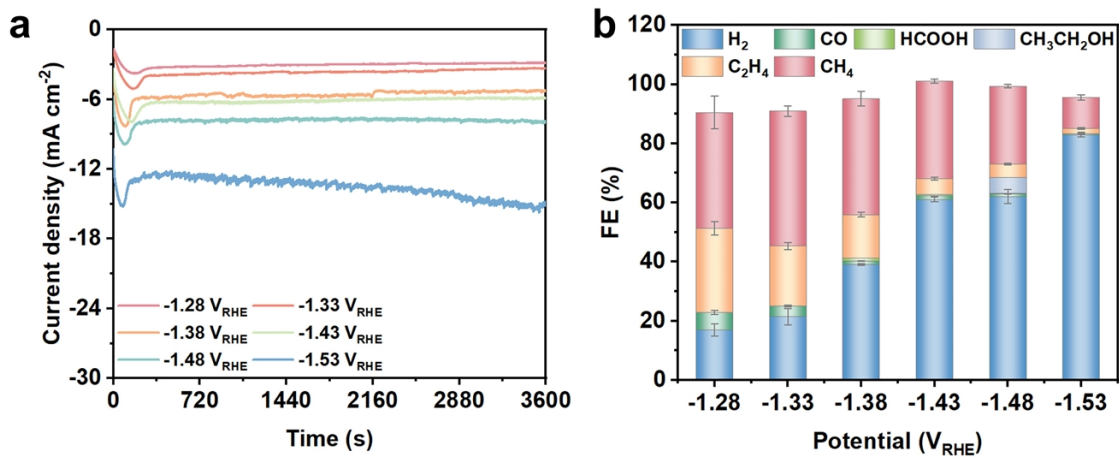
106 **Fig. S8** (a) Total current density at various applied potentials for CuO. (b) Total current density at
 107 various applied potentials for Eu/Cu-2.

108



109

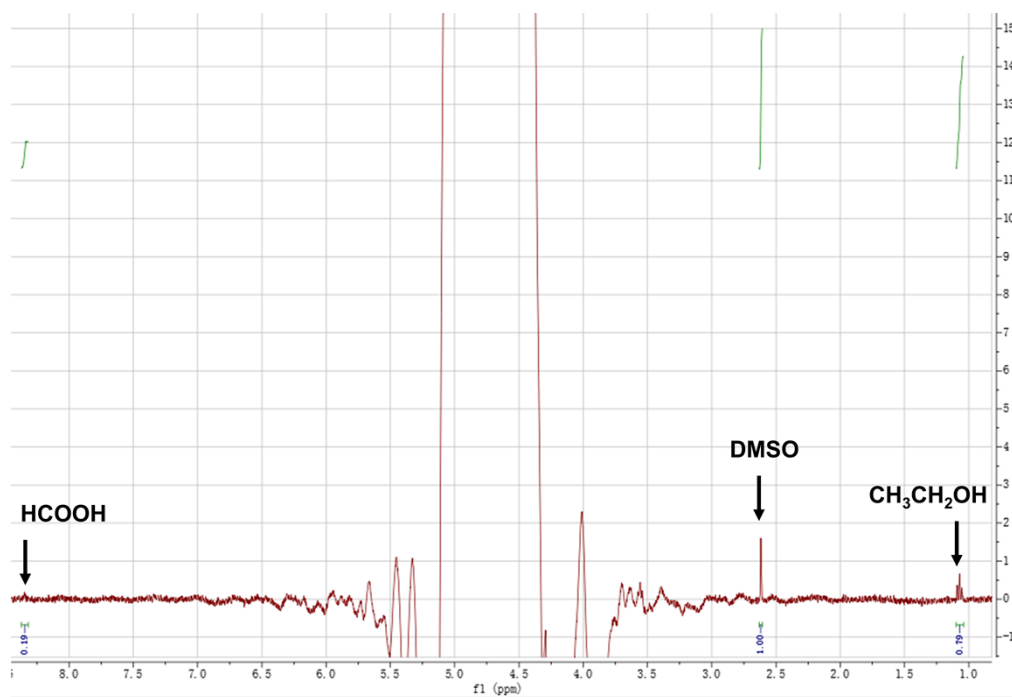
110 **Fig. S9** (a) Total current density at various applied potentials for Eu/Cu-1. (b) FE of Eu/Cu-1 at
 111 various applied.



112

113 **Fig. S10** (a) Total current density at various applied potentials for Eu/Cu-3. (b) FE of Eu/Cu-3 at

114 various applied potential.

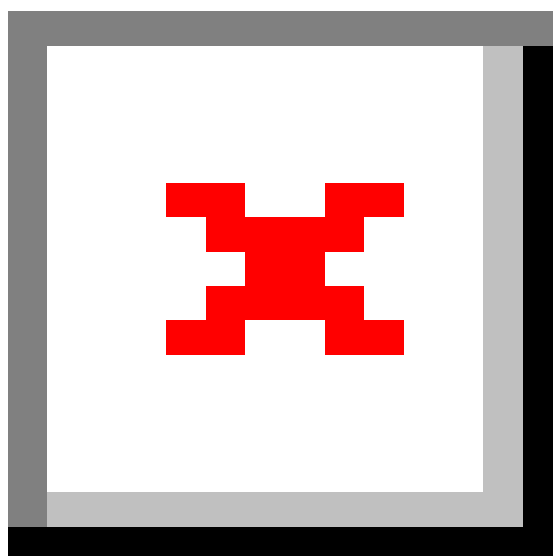


115

116

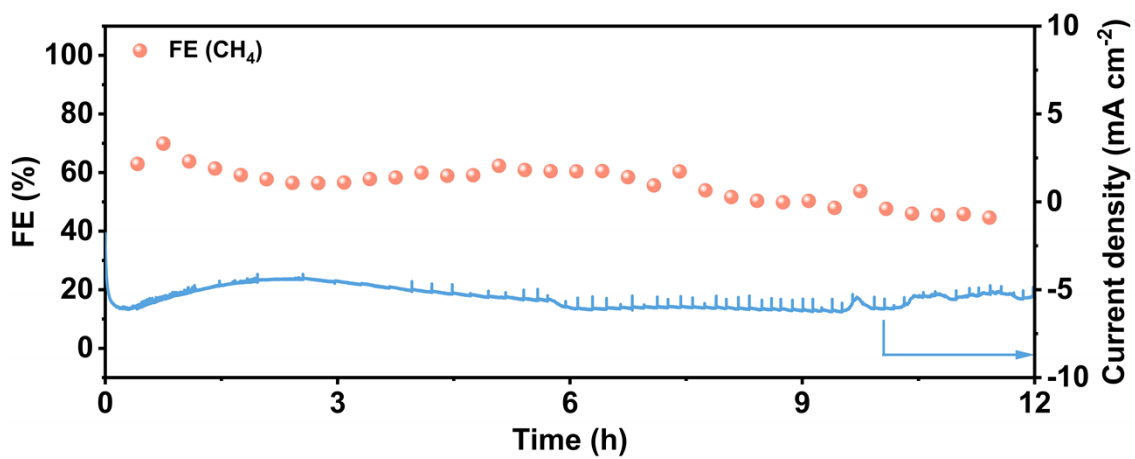
117

Fig. S11 ^1H NMR analysis of liquid products.



118

119 **Fig. S12** Performance comparison of Eu/Cu-2 with representative Cu-based catalysts for CO₂
120 reduction to CH₄.

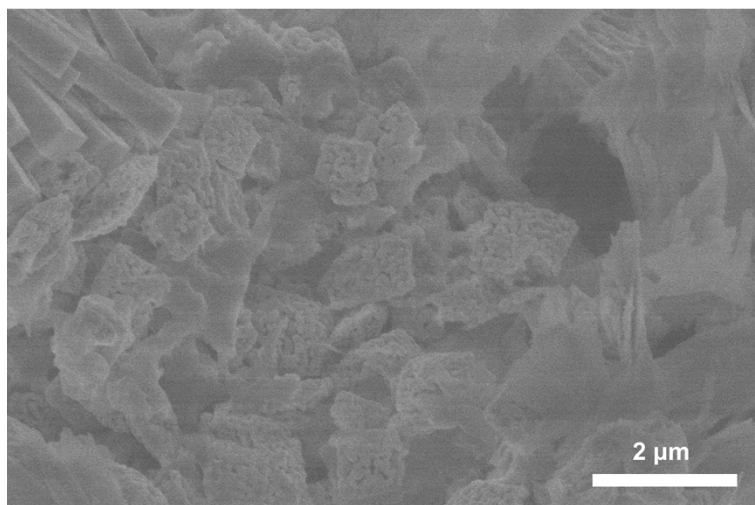


121

122

Fig. S13 Stability measurement of Eu/Cu-2 within 12 h.

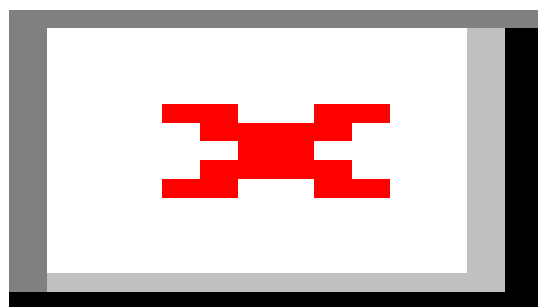
123



124

125

Fig. S14 SEM after 12h electrolysis of Eu/Cu-2.

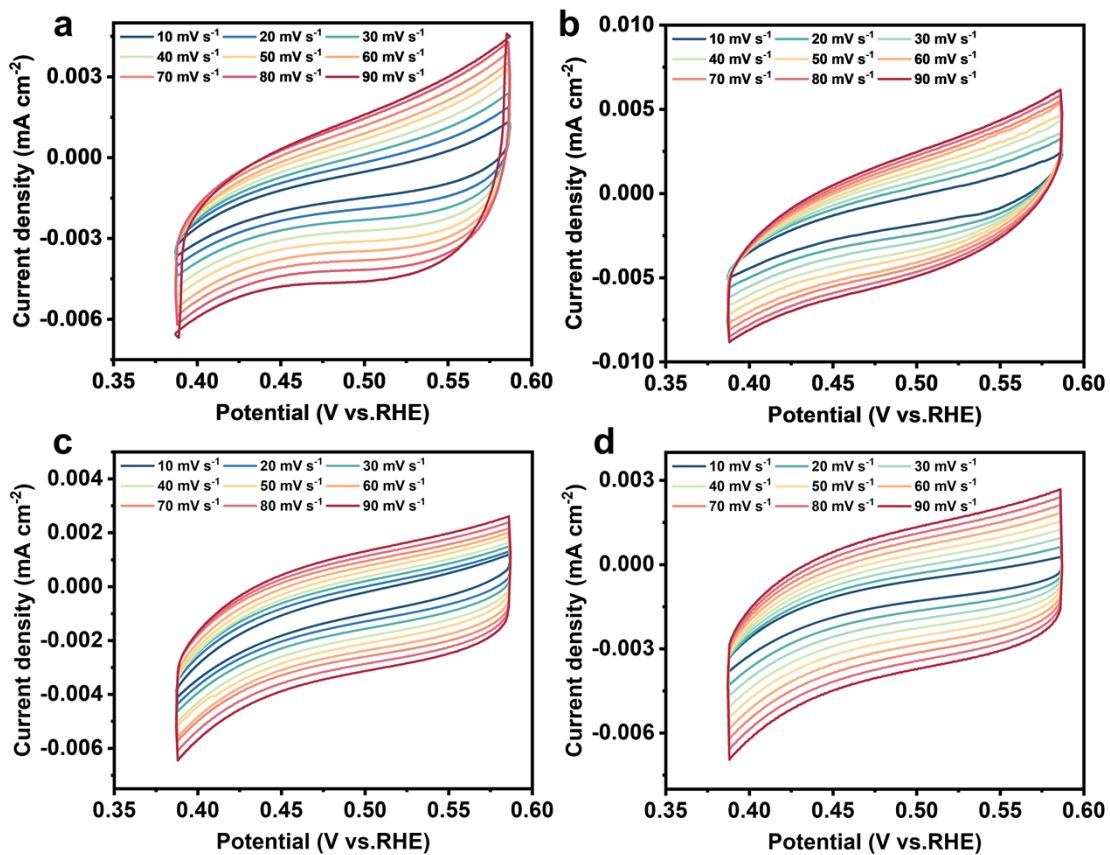


126

127

128

Fig. S15 Stability measurement of CuO within 5 h.

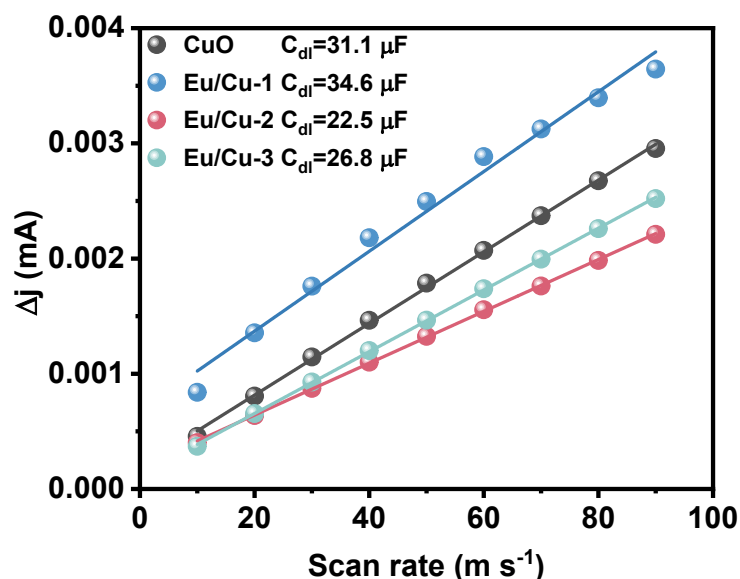


129

130 **Fig. S16** Electrochemical surface area (ECSA) measurement of the true catalyst after electrolysis.

131 (a-d) cyclic voltammetry (CV) with various scan rates for CuO, Eu/Cu-1 Eu/Cu-2 and Eu/Cu-3 after
 132 electrolysis.

133



134

135 **Fig. S17** Current due to double-layer charging plotted against CV scan rate for CuO, Eu/Cu-1 Eu/Cu-
 136 2 and Eu/Cu-3 after electrolysis.

137

138 **Note:** The ECSA was determined by analyzing the non-Faradaic capacitive current associated with
 139 double-layer charging, as demonstrated through cyclic CV scan rate dependence. For details, CV
 140 measurements were performed within a non-Faradaic potential window of -0.70 to 0.95 V_{RHE}, with
 141 scan rates ranging from 10 to 100 mV s⁻¹. The double-layer capacitance (C_{dl}) was calculated by

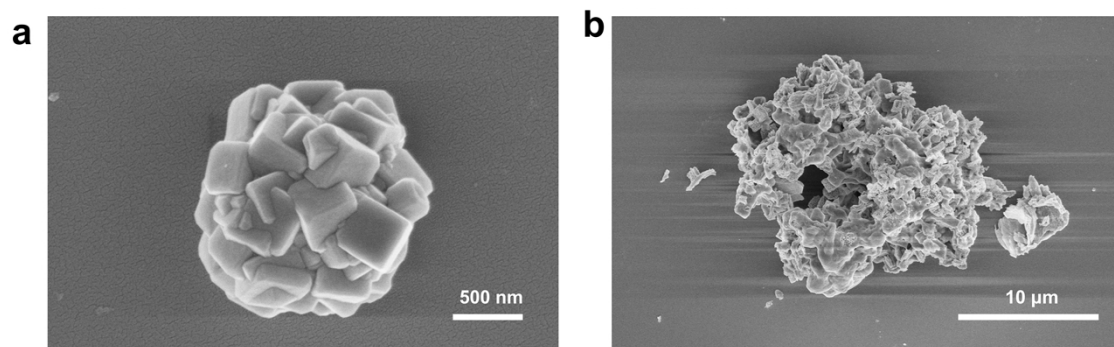
142 plotting $\frac{\Delta j}{2} = \frac{(j_a - j_c)}{2}$ at 0 V_{RHE} against the scan rate. The linear slope of this plot corresponds to C_{dl} ,
 143 which is proportional to the ECSA. The ECSA was then calculated using the equation:

$$ECSA = \frac{C_{dl}}{C_s}$$

144

145 where C_s is the specific capacitance. We use a typical C_s value of 0.04 mF cm⁻² based on previous
 146 reports.¹ The calculated ECSA values were 0.778, 0.865, 0.563, 0.67 for CuO, Eu/Cu-1 Eu/Cu-2 and
 147 Eu/Cu-3, respectively. The calculated ECSA values were 22.48, 13.54, 8.795, 10.40 cm² for CuO,
 148 Eu/Cu-1 Eu/Cu-2 and Eu/Cu-3, respectively. The slightly lower ECSA of Eu/Cu-2 may be attributed
 149 to its relatively larger particle size.

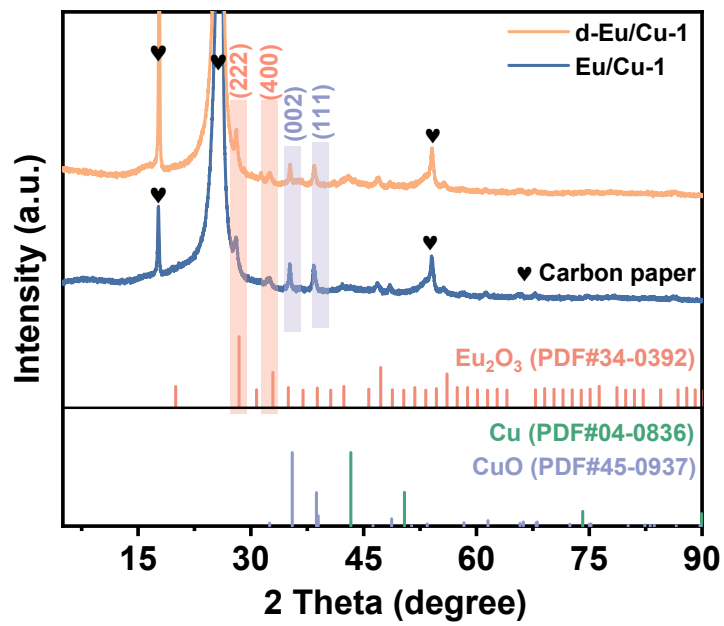
150



151

152

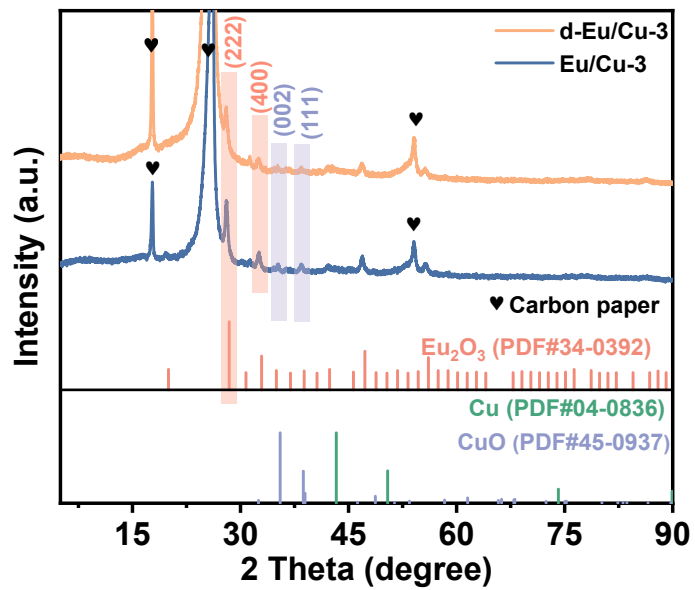
Fig. S18 (a) SEM of d-CuO. (b) SEM of d-Eu/Cu-2



153

154

Fig. S19 XRD pattern of d-Eu/Cu-1 and Eu/Cu-1.



155

156

Fig. S20 XRD pattern of d-Eu/Cu-3 and Eu/Cu-3.

157 **3. Supplementary Table**

158 **Table S1.** Performance comparison of Eu/Cu-2 with representative Cu-based catalysts for CO₂
 159 reduction to CH₄. (corresponding to Fig. S12).

Catalyst	Applied Potential	Electrolyte	FE (%)	Ref
Eu/Cu-2	-1.38 V _{RHE}	0.1 M KCl	63.1%	This work
La ₂ CuO ₄ perovskite	-1.4 V _{RHE}	0.1 M KHCO ₃	56.3%	2
Cu-Pd heterostructure	-1.25 V _{RHE}	0.1 M KHCO ₃	32%	3
Pd-decorated Cu	-0.96 V _{RHE}	0.5 M KHCO ₃	46%~40%	4
Concave rhombic dodecahedral Cu ₃ Pd	-1.2 V _{RHE}	0.1 M KHCO ₃	40.6%	5
Cu nanowires/rGO	-1.25 V _{RHE}	0.5 M KHCO ₃	55%	6
Cu NPs derived from MOFs	-1.3 V _{RHE}	0.1 M KHCO ₃	≈50%	7
CuS@Ni Foam	-1.1 V _{RHE}	0.1 M KHCO ₃	73%	8
Au@Cu core@shell nanoparticles)	-0.6 V _{RHE}	PBS (pH = 8)	≈20%	9
Cu ₂ Pd nanoalloy	-1.8 V _{Ag/AgNO₃}	0.1 M KHCO ₃	51%	10
Cu-Pt (3:1) nanocrystal	-1.8 V _{SCE}	0.5 M KHCO ₃	21%	11
Cu electrodeposition on Pt disk	-2.23 V _{Ag/AgCl}	0.1 M KHCO ₃	60%	12
Electrodeposited polycrystal Cu-GDE	-2.23 V _{Ag/AgCl}	0.5 M KHCO ₃	52%	13
Electropolished Cu(210) single crystal	-1.8 V _{SCE}	0.1 M KHCO ₃	64%	14

160

161 **References**

162 1. R. Appiah-Ntiamoah and H. Kim, *J. Colloid Interface Sci.*, 2022, **606**, 607-617.

163 2. S. Chen, Y. Su, P. Deng, R. Qi, J. Zhu, J. Chen, Z. Wang, L. Zhou, X. Guo and B. Y. Xia, *ACS*

- 164 *Catal.*, 2020, **10**, 4640-4646.
- 165 3. J.-F. Xie, J.-J. Chen, Y.-X. Huang, X. Zhang, W.-K. Wang, G.-X. Huang and H.-Q. Yu, *Appl.*
166 *Catal., B*, 2020, **270**, 118864.
- 167 4. Z. Weng, X. Zhang, Y. Wu, S. Huo, J. Jiang, W. Liu, G. He, Y. Liang and H. Wang, *Angew.*
168 *Chem. Int. Ed.*, 2017, **56**, 13135-13139.
- 169 5. W. Zhu, L. Zhang, P. Yang, X. Chang, H. Dong, A. Li, C. Hu, Z. Huang, Z.-J. Zhao and J. Gong,
170 *Small*, 2018, **14**, 1703314.
- 171 6. Y. Li, F. Cui, M. B. Ross, D. Kim, Y. Sun and P. Yang, *Nano Lett.*, 2017, **17**, 1312-1317.
- 172 7. P. Chen, Y. Jiao, Y.-H. Zhu, S.-M. Chen, L. Song, M. Jaroniec, Y. Zheng and S.-Z. Qiao, *J.*
173 *Mater. Chem. A*, 2019, **7**, 7675-7682.
- 174 8. Z. Zhao, X. Peng, X. Liu, X. Sun, J. Shi, L. Han, G. Li and J. Luo, *J. Mater. Chem. A*, 2017, **5**,
175 20239-20243.
- 176 9. J. Monzó, Y. Malewski, R. Kortlever, F. J. Vidal-Iglesias, J. Solla-Gullón, M. T. M. Koper and P.
177 Rodriguez, *J. Mater. Chem. A*, 2015, **3**, 23690-23698.
- 178 10. S. Zhang, P. Kang, M. Bakir, A. M. Lapides, C. J. Dares and T. J. Meyer, *Proc Natl Acad Sci U*
179 *SA*, 2015, **112**, 15809-15814.
- 180 11. X. Guo, Y. Zhang, C. Deng, X. Li, Y. Xue, Y.-M. Yan and K. Sun, *Chem. Commun.*, 2015, **51**,
181 1345-1348.
- 182 12. O. A. Baturina, Q. Lu, M. A. Padilla, L. Xin, W. Li, A. Serov, K. Artyushkova, P. Atanassov, F.
183 Xu, A. Epshteyn, T. Brintlinger, M. Schuette and G. E. Collins, *ACS Catal.*, 2014, **4**, 3682-3695.
- 184 13. D. Kim, S. Lee, J. D. Ocon, B. Jeong, J. K. Lee and J. Lee, *Physical Chemistry Chemical Physics*,
185 2015, **17**, 824-830.
- 186 14. Y. Hori, I. Takahashi, O. Koga and N. Hoshi, *J. Mol. Catal. A: Chem.*, 2003, **199**, 39-47.
- 187